Electrical properties of He-implantation-produced nanocavities in silicon

C. H. Seager, S. M. Myers, R. A. Anderson, W. L. Warren, and D. M. Follstaedt
Sandia National Laboratories, Albuquerque, New Mexico 87185
(Received 20 December 1993; revised manuscript received 6 April 1994)

When silicon implanted with $> 10^{16}$ He cm^{-2} is annealed at 700 °C or above, the He forms bubbles and then diffuses out leaving voids (nanocavities). We have prepared *n*-type and *p*-type Si samples with nanocavity layers and characterized their structure and their effect on the local band structure and the transport of charge. The ambipolar Si dangling orbitals at the nanocavity walls trap majority carriers in both types of silicon and form quasi-one-dimensional potential barriers which impede transport of charge across the cavity layer. Using dc conductance and high-frequency capacitance techniques we have characterized the height and width of these electrostatic barriers. Capacitance measurements have also been employed to study the evolution of trapped dangling-bond charge as the void containing layers are depleted of carriers in *n*-type and *p*-type Schottky-barrier structures. With transient capacitance techniques we have characterized the emission of holes from the unoccupied dangling-bond localized states and also the emission of electrons from the doubly occupied states. The lower dangling-bond level is 0.17 eV above the valence-band maximum, while the upper level lies 0.38 eV below the conduction-band minimum; these energies are qualitatively consistent with broader spectral features observed in ultrahigh-vacuum photoemission experiments on clean reconstructed Si surfaces. Electron paramagnetic resonance (EPR) has been employed to observe unpaired spins associated with dangling orbitals on the cavity walls. The strength of the EPR signal corresponds to ~ 0.1 unpaired spin per dangling orbital, and this reduced amplitude is interpreted in terms of charge redistributions among inequivalent sites which are well known to occur on reconstructed Si surfaces. A simple, one-electron model yields semiquantitative agreement with much of the experimental data on electrical properties and helps explain some of the unusual emission-rate prefactors seen in the capacitance-transient experiments. We nevertheless conclude that a more realistic treatment, including electron-electron repulsion within the cavities as well as charge redistributions on the neutral surface, is probably needed for quantitative prediction.

I. INTRODUCTION

It has been recognized for some time that ion implantation of He into Si produces bubbles, and that subsequent annealing at temperatures above 700 °C causes the He to diffuse out of the material leaving voids.[1] The walls of these nanocavities are believed to be pristine surfaces, and recently, several of their properties have been investigated. The dissociation energy of the Si-H surface bond, which has proved inaccessible to ultrahigh-vacuum experiments on external Si surfaces, was determined from studies of H on the cavity surfaces.[2–4] The transition-metal solute Cu was shown to be strongly trapped by the internal surfaces,[5] raising the possibility of using cavities for impurity gettering in Si devices. Finally, an analysis of equilibrium faceting in cavities yielded the relative free energies of the low-index surfaces of Si.[6,7]

In the present paper, we report an investigation of the electrical properties of internal cavity surfaces in Si. The electronic states associated with dangling bonds on external, neutral surfaces have previously been examined using scanning tunneling microscopy, photoemission, and inverse-photoemission spectroscopies; these reveal states in the band gap corresponding to occupation of the dangling orbitals by zero, one, and two electrons.[8] In the present investigation, we are concerned instead with surfaces that have nonzero net charge and that are located within the bulk Si matrix. When the surface lies at micrometer depths within the Si, a different array of powerful electrical diagnostics can be brought to bear on the dangling-bond states; these include conductivity, capacitance versus voltage, deep-level transient spectroscopy (DLTS), and electron paramagnetic resonance (EPR) techniques. Such measurements were performed in the present study to complement the information from external-surface experiments. Additionally, we sought to determine the effects of cavity-containing layers on the electrical properties of doped Si to facilitate the exploitation of these layers in devices for such purposes as impurity gettering and electrical isolation.

II. EXPERIMENTAL METHODS

A. Sample preparation

Four different types of samples were employed in this study. While the implantation and annealing schedule employed to create the nanocavities were identical for all four, the doping type and contacting procedures varied from sample to sample. (a) *Ohmically contacted p-type samples.* These were fabricated from 7–13 Ω cm, boron doped, Czochralski-grown ⟨111⟩ silicon which had been heavily B implanted on the unpolished back side for ohmic contact formation. After a 300-keV, 1×10^{17}-cm^{-2} He implant and a 900-°C, 1-h vacuum anneal to form the nanocavities, these samples were etched in buffered oxide

etch for 20 sec and rinsed in deionized water. This was followed by the evaporation of 300 Å of Al on both the front and back sides. The front electrode (on the He-implanted side) was almost as large ($\sim 95\%$) as the entire sample area. These samples were then annealed at 450 °C for 20 min in air to produce good low-resistance contacts on both sides of the samples. (b) *Schottky-barrier p-type samples.* These samples were fabricated from 3–6 Ω cm boron doped silicon and were He implanted and annealed as above. The back contact procedure was the same as for the Ohmic samples (above), but the front Al metallizations were evaporated after the 450-°C, 20-min anneal in air. The thin (20–30 Å) SiO_2 layer beneath this metal insured that a high-resistance Schottky-type contact was established. (c) *Ohmically contacted n-type samples.* These samples were made from phosphorus-doped ⟨100⟩ material of nominal resistivity 0.8–1.2 Ω cm. In addition to the above front side He implant, both sides were also implanted with phosphorus at 30 keV to a dose of 2×10^{14} cm^{-2} followed by a 900-°C, 1-h vacuum anneal to produce the nanocavities and activate the P implant. Ohmic metallizations were made on these heavily doped layers by sputtering ~ 130 Å of Au through a shadow mask. (d) *n-type Schottky barriers.* These samples were fabricated in the same fashion as the *n*-type ohmically contacted samples, but in this case we employed 5–10 Ω cm ⟨100⟩ silicon with no front side phosphorus implant.

B. Sample characterization

The cavity microstructure produced by He ion implantation and subsequent annealing at 900 °C is shown in the cross-section TEM micrograph of Fig. 1. To facilitate cross-sectional thinning, the implantation energy for the TEM specimen was reduced from 300 to 30 keV, thereby shifting the average depth of the cavities from about 1.35 μm to the approximately 0.3 μm seen in the micrograph. This reduction in energy also reduced somewhat the calculated range spread of the implanted He, causing the predicted peak concentration for the implantation fluence of 1×10^{17} He/cm^2 to increase from about 7 to 9 at. %. This difference is believed to be inconsequential for the purposes of this paper. Detailed analysis of a series of micrographs yielded the following parameters relevant to the consideration of electrical properties: average cavity diameter $=18$ nm, areal density of cavities $=3.1\times10^{11}$ cm^{-2}, and calculated number of internal-surface dangling bonds per unit sample area $=2.6\times10^{15}$ cm^{-2}. The last of these values is consistent with the numbers of H and Cu atoms that have been observed to bind to the cavity walls in separate studies.[2–5]

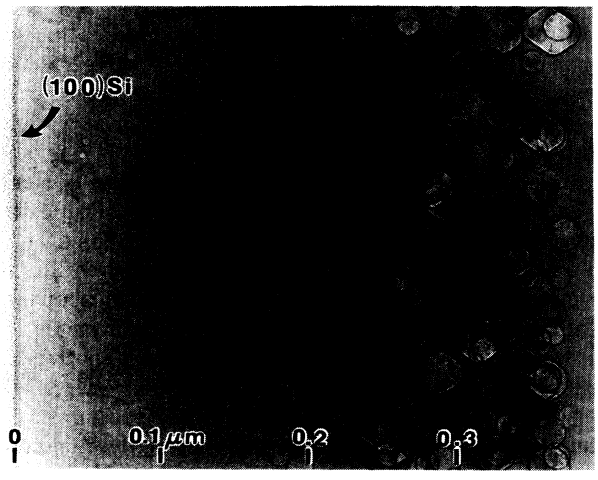

FIG. 1. Cross-sectional ⟨011⟩ TEM micrograph of a (100) silicon sample which has had a 1×10^{17} atoms/cm^2, 30-keV He implant followed by a 900 °C, 1/2 h vacuum anneal. The specimen was tilted to reduce diffraction contrast and imaged at −600 nm under focus to enhance the contrast of the cavities. Clear evidence of faceting is seen.

Some dislocations with residual contrast are also seen in the micrograph of Fig. 1. In separate TEM analysis the dislocations were imaged with better contrast, and the following properties were thereby obtained: line areal density $=1.3\times10^6$ cm/cm^2, core-atom areal density $\sim 5\times10^{13}$ cm^{-2}, kink areal density $=1.5\times10^{11}$ cm^{-2} (all expressed per front surface wafer area). It thus appears that the number of dangling bonds associated with the dislocations is 2–4 orders of magnitude smaller than those on internal cavity surfaces, depending on the degree of dimerization of broken bonds in the dislocation cores. Therefore, since point defects are not expected to be present in significant numbers after annealing at 900 °C, the electrical effects reported in this paper are ascribed to the cavities.

The cavity-containing Si was also examined by EPR, a probe that is specifically sensitive to the neutral, paramagnetic state of the Si dangling bond. The EPR measurements were performed at either 20 or 300 K using a Bruker ESP-300 E X-band spectrometer. The spectrum obtained at a temperature of 20 K is shown in Fig. 2. Also shown for comparison are data from three control samples that had been respectively treated as follows: (1) not ion-implanted but annealed for 1 h at 900 °C as was the cavity-containing material; (2) pre-anneal He-implantation step replaced by proton implantation at 155 keV and the lower fluence of 10^{16} cm^{-2} to introduce displacement damage without cavity formation; (3) H passivated after cavity formation by heating in H_2 gas at 87 kPa pressure and 700 °C for 24 h. In addition to these controls, the first specimen was remeasured after its cavity layer had been chemically removed, and, as expected, the EPR signal reverted to that of the background.

In combination, the above EPR results indicate the presence of a relatively small background signal from the Si bulk together with a cavity-associated signal that is subject to high-temperature H passivation. The cavity resonance has a g value of 2.0057, a width of 11.9 G, and is isotropic with respect to magnetic-field orientation. This resonance is similar to that ascribed to dangling bonds[9] in *a*-Si, but has almost twice the linewidth. The apparent areal density of spins is 8×10^{13} cm^{-2} with a factor-of-2 uncertainty, or about an order of magnitude smaller than the number of surface atoms deduced from TEM and from H and Cu surface reactions. We believe that this cavity-associated electron spin resonance signal

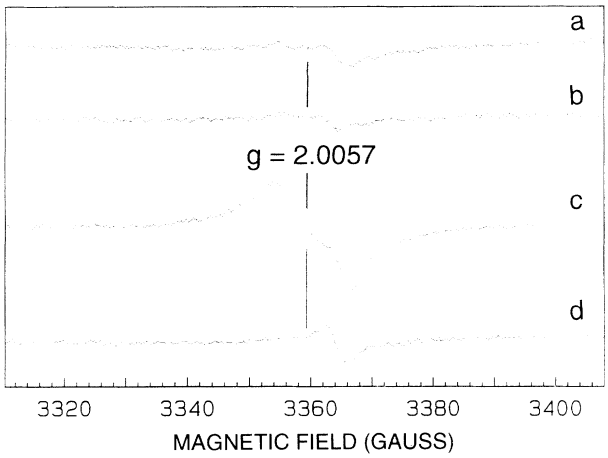

FIG. 2. Electron paramagnetic resonance spectra measured at 20 K on high-resistivity silicon samples. Sample *a* was unimplanted but had a 900-°C vacuum anneal. Sample *b* was implanted with protons at an energy of 155 keV and 900-°C vacuum annealed. Sample *c* had a 10^{17}-cm^{-2} 300-keV He implant followed by a 900-°C vacuum anneal, producing cavities as seen in Fig. 1. Sample *d* was prepared identically to sample *c*, but had a final 24-h passivation anneal in 87 kPa of H_2 at 700 °C.

qualitatively supports the existence of Si dangling bonds on the internal surfaces. The reduced amplitude is hypothesized to result from charge transfers among structurally inequivalent dangling-bond sites, which would have the effect of diminishing the effective density of unpaired spins. Such charge redistributions on the reconstructed neutral surfaces of Si are well known from both experimental and theoretical work.[8]

C. Electrical measurements

The electrical properties of the nanocavities were determined by standard techniques. Currents through the ohmically contacted samples were measured with a Keithly 619 digital electrometer with voltages supplied by a Keithley 230 programmable voltage source. All capacitance determinations were made in a three terminal mode on either Boonton 72B (at 1 MHz) or Boonton 72C (at 100 kHz) capacitance bridges. The analog outputs of these bridges were fed to a Nicolet digital oscilloscope which recorded capacitance versus time in the transient experiments. External dc bias to the Boonton bridges was provided by the Keithley 230 voltage source.

During all of the electrical measurements the samples were located in the dark in a UHV capable vacuum chamber with typical (unbaked) chamber pressures of 4×10^{-5} Pa. Temperature measurement was made with a calibrated Chromel-Alumel thermocouple spot welded to the sample holding platform.

III. THEORETICAL MODELING

The experiments chosen for this study were motivated by prior results of surface spectroscopies on surface Si dangling orbitals and by experience with analogous systems of charged defect layers such as Si grain boundaries. In order to present our results in coherent fashion, we will first anticipate some of the electronic properties that these cavity layers might possess and review our semiquantitative modeling of the band structure near these layers and the effect they have on the transport of electronic carriers.

We expect that surface Si dangling bonds will have an ambipolar character; that is they possess positive (donorlike) and negative (acceptorlike) charge states, depending on the position of the Fermi level in the forbidden gap. This behavior has been verified for dangling Si orbitals on reconstructed Si surfaces *in vacuo*,[8] for Si-related states at the Si/SiO_2 interface (the so-called P_{b0} and P_{b1} centers),[10–12] and for the apparently intrinsic states present at "clean" Si grain boundaries[13] and dislocations.[14] A simple consequence of this is that these defects will trap majority carriers in both *n*-type and *p*-type silicon, producing a repulsive band bending that prevents further charging. These charge accumulations are seen at dislocations where they represent line charge, and grain boundaries where they exist as areal charge. In the latter case, which is somewhat analogous to the present situation, their effects on the transport of majority carriers across the boundary are substantial, since they may bend the bands as much as 0.3 to 0.4 eV.[15]

We further anticipate that silicon with a layer of nanocavities will exhibit complicated electrical behavior because: (1) the internal-surface Si dangling bonds have positive, neutral, and negative charge states which produce deep levels[8] in the band gap, (2) the small distance between dangling bonds leads to strong Coulomb interactions among the charged states, and (3) the depth distribution of the cavities is nonuniform. Therefore, in order to examine the link between cavity-related electronic states and the electrical behavior observed in the present studies, we have theoretically examined the behavior of a simplified model system. In this model, the Si contains a uniform concentration of B or P dopants together with cavity-associated localized donor and acceptor states distributed in depth according to the calculated depth distribution of implanted He. This calculation was performed using a TRIM code,[16] yielding a concentration curve which peaks at a depth of 1.35 μm with a $\sim$0.25 μm width at half maximum. The [+/0] and [0/−] transitions of the dangling bonds are treated as if they occur independently, an acceptable simplification if the positive and negative states are not substantially occupied at the same time. The number of dangling bonds within the He-implanted Si is believed to correspond to about one monolayer on the internal surfaces, but we anticipate that the number of positive or negative charges is limited to a much smaller value by Coulomb repulsion between sites located on the same cavity. In the present model, we simulate this effect to first order by making the number of cavity-associated donors and acceptors equal to 1 per cavity (which is $\sim10^{-4}$ times the number of dangling bonds) and then assigning a large degeneracy to the charged states to take account of the multiplicity of dangling-bond sites within a typical nanocavity. At small charge occupations, this approach yields approximately the same results as equating the localized acceptor and

donor densities with the dangling-bond density, but it has the advantage of limiting charge occupation to one electron and/or one hole per cavity, thus addressing Coulomb repulsion effects. More elaborate calculations of nanocavity charge occupation treating Coulomb interactions with mean-field theory have been carried out, but will not be presented here; they yield results that do not differ drastically from those of the simplified model. We also note that our treatment does not include the effects of Peierl's distortions which asymmetrize otherwise equivalent dangling bonds. As an example, these relaxations result in "buckled dimers" and charge transfer on Si(001) 2×1 surfaces.[8] While they must have strong effects on the nanocavity paramagnetism, no attempt has been made to quantitatively include them in our description of the charging of these layers.

Our mathematical treatment of the above model system uses established methods and, for the most part, conventional notation.[17,18] The central task is the solution of Poisson's equation,

$$(d^2/dx^2)V(x)=-\rho(x)/\varepsilon \ , \tag{1}$$

where V is the electrostatic potential, ρ is the net charge density, and ε is the permittivity of Si. The densities of conduction electrons and of holes contributing to the charge density are given respectively by

$$n(x)=N_C\exp\{[E_{F,n}(x)-E_C(x)]/kT\} \tag{2}$$

and

$$p(x)=N_V\exp\{[E_V(x)-E_{F,p}(x)]/kT\} \ , \tag{3}$$

where N_C is the effective density of states in the conduction band, $E_{F,n}$ is the electron quasi-Fermi level, E_C is the energy of the conduction-band edge, N_V is the effective density of states in the valence band, E_V is the valence-band edge, and $E_{F,p}$ is the hole quasi-Fermi level. The band edges are functions of depth due to the varying electrostatic potential, which shifts both E_V and E_C by the amount $-qV(x)$. The fraction of localized donor states of a given type that are positively charged under steady-state conditions is

$$f_{\rm don}(x)=[p(x)v_{\rm th}\sigma_{p,\rm don}+e_{n,\rm don}]\tau_{\rm don}(x) \ , \tag{4}$$

while the fraction of negatively charged accceptor states is

$$f_{\rm acc}(x)=[n(x)v_{\rm th}\sigma_{n,\rm acc}+e_{p,\rm acc}]\tau_{\rm acc}(x) \tag{5}$$

with

$$\tau(x)\equiv[p(x)v_{\rm th}\sigma_p+e_n+n(x)v_{\rm th}\sigma_n+e_p]^{-1} \ , \tag{6}$$

where $v_{\rm th}$ is the carrier thermal velocity, σ is the capture cross section for an electron or hole, and e is the emission rate for an electron or hole. The quantity $\tau(x)$ is a characteristic time for the decay of small departures from steady state and is evaluated separately for the donor or acceptor dangling-bond level by substituting appropriate values of σ_p or σ_n into Eq. (6). Consideration of detailed balance under equilibrium conditions, with the assumption that the charged states of the localized acceptors and donors have an effective degeneracy of α, indicates that

$$e_{n,\rm don}=v_{\rm th}\sigma_{n,\rm don}N_C\exp[(E_t-E_C)/kT]\alpha \ , \tag{7}$$

$$e_{n,\rm acc}=v_{\rm th}\sigma_{n,\rm acc}N_C\exp[(E_t-E_C)/kT]/\alpha \ , \tag{8}$$

$$e_{p,\rm don}=v_{\rm th}\sigma_{p,\rm don}N_V\exp[(E_V-E_t)/kT]/\alpha \ , \tag{9}$$

and

$$e_{p,\rm acc}=v_{\rm th}\sigma_{p,\rm acc}N_V\exp[(E_V-E_t)/kT]\alpha \ , \tag{10}$$

where E_t is the position of the donor or acceptor level in the band gap.

The quasi-Fermi levels for electrons and holes are treated in one of three ways depending on circumstances.[17,18] In equilibrium, one has $E_{F,n}=E_{F,p}\equiv E_F=$constant, with the value of E_F being determined by the requirement of charge neutrality at $x=\infty$ in the semiconductor. For the case of a Schottky diode under reverse bias, a simple and usually acceptable approach is to assume that both quasi-Fermi levels are independent of depth in the depleted zone, with the majority-carrier level joining the semiconductor Fermi level at $x=\infty$, and the minority-carrier level matching the Fermi level in the overlying metal. This approximation conforms to the "thermionic-emission theory," where the majority carrier current is assumed to be limited solely by the transfer of charge over the Schottky barrier. In selected cases we refine this treatment by solving a continuity equation for the majority-carrier current, which then determines the majority-carrier quasi-Fermi level as a function of depth. The continuity equation for electrons in the absence of carrier annihilation is

$$q\mu_n n(x)(d/dx)E_{F,n}(x)=-A^*T^2\exp(-\phi_{b,n}/kT)(1-\exp\{[E_{F,n}(x=0)-E_{F,\rm met}]/kT\}) \ , \tag{11}$$

while that for holes is

$$q\mu_p p(x)(d/dx)E_{F,p}(x)=A^*T^2\exp(-\phi_{b,p}/kT)(1-\exp\{[E_{F,\rm met}-E_{F,p}(x=0)]/kT\}) \ , \tag{12}$$

where q is the magnitude of the electron charge, μ is the carrier mobility, A^* is the effective Richardson constant, ϕ_b is the amplitude of the Schottky barrier, and $E_{F,\rm met}$ is the Fermi level in the metal. These equations are obtained by equating the migration current at depth x in the depletion zone to the emission current over the barrier. Since they contain the depth-dependent carrier concentration as well as the quasi-Fermi level, they must be solved simultaneously with Eq. (1). This more elaborate approach is generally referred to[17] as the "combined thermionic-emission/diffusion theory."

Equation (1) is solved numerically by integrating in-

ward from the surface with specified values of $V(x=0)$ and $(d/dx)V(x)|_{x=0}$. At each of a succession of depths x_i, the quantities V and $(d/dx)V$ are first evaluated using the values of V, $(d/dx)V$, and $(d^2/dx^2)V$ at x_{i-1}. The local charge ρ is then determined from Eqs. (2)–(10), which then yields the second derivative $(d^2/dx^2)V$ at depth x_i through the use of Eq. (1). Since $(d/dx)V(x)|_{x=0}$ is not independently known, its value is varied to achieve charge neutrality deep within the specimen, $\rho(x=\infty)=0$. In those cases where Eq. (11) or (12) is solved simultaneously with Eq. (1), the quasi-Fermi level at x_i is evaluated from its value and first derivative at x_{i-1}. The value at $x=0$ is not independently known, and it is, therefore, varied to achieve coincidence with the semiconductor Fermi level at $x=\infty$. In order to achieve reliable convergence of the solution under widely varying conditions and in the presence of an extremely sensitive and highly nonlinear relationship between V and ρ, we use the somewhat inefficient but robust method of testing the entire ranges of plausible values for $(d/dx)V(x)|_{x=0}$, $E_{F,n}(x=0)$, and $E_{F,p}(x=0)$, moving the test values in increments that decrease by one half from one step to the next. Detailed calculations using the above approach will be examined in Sec. III after the experimental results are discussed below.

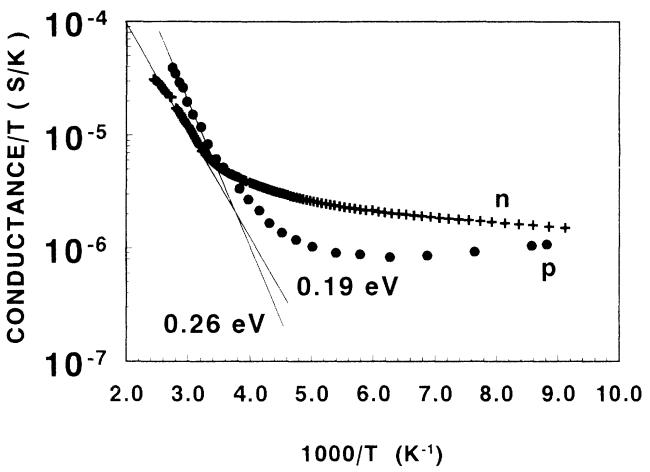

FIG. 3. Conductance divided by absolute temperature versus inverse temperature for ohmically contacted n-type (crosses) and p-type (circles) Si samples containing a buried layer of He-implantation-produced nanocavities. The sample electrode areas were 11.6 mm^2. At higher temperatures the conductance is strongly activated, reflecting the potential barrier associated with band bending. At lower temperatures the variation is much weaker, and this is tentatively ascribed to isolated regions of reduced cavity density where the potential barrier is smaller.

IV. ELECTRICAL TRANSPORT DATA

A. Conductance measurements

We now examine the experimental data for the ohmically contacted samples to look for evidence of charge accumulation at the nanocavities. The most straightforward test for this is to measure the impedance it offers to majority carrier flow. Given the resistivity level for the present samples (7–13 Ω cm for the p-type and 0.8–1.2 Ω cm for the n type), we would expect that the resistance offered by the Si bulk would be at most a few ohms in our sample configuration. The observed conductances (divided by absolute temperature) of the n-type and p-type nanocavity samples at low bias (~0.01 V) are shown versus $1000/T$ in Fig. 3, respectively. The conductance values observed here are quite low at room temperature (~0.003 S), they follow an Arrhenius temperature dependence above ~300 K, and show a weakening T dependence at lower temperatures. The behavior seen at higher temperatures is that expected for thermionic emission of majority carriers over a uniform potential barrier whose height (measured from the equilibrium Fermi level) can be reduced from the activation energy shown on these plots. That is, for n-type silicon, we expect[19]

$$G=(A^*T^2/k)\exp\{-(\phi_B+\zeta)/kT\}[(1-e^{-qV_a/kT})/V_a], \tag{13}$$

where ϕ_B is the electrostatic band bending at the top of the nanocavity-associated electrostatic barrier, ζ is the energy difference between the Fermi level and the conduction band bottom, and V_a is the applied bias. An analogous expression holds for the p-type case. Since the $V_a=0$ limit of the square brackets in Eq. (13) is q/kT, we expect that G/T should show a thermally activated, Arrhenius dependence at low biases. In Fig. 3, the flattening of the plots at low temperatures is not expected from Eq. (13) and will be discussed in Sec. V.

B. Zero-bias capacitance measurements

A second test for the presence of potential barriers in these samples is to see if these charged structures show the type of capacitance that we expect for depletion barriers. It has been shown[20] that at frequencies high enough that charge cannot be captured or emitted by localized states in a barrier, the capacitance of such potential barriers simply reflects their width via the parallel-plate expression

$$C_{hf}=A\varepsilon/w\ , \tag{14}$$

where A is the sample area and w is a measure of the depletion width surrounding the nanocavities (see Fig. 3). In Fig. 4, we plot the depletion layer widths deduced from this formula and 1-MHz capacitance measurements on n-type and p-type ohmically contacted samples. The calculated w values are larger for the p-type sample, which is more weakly doped than the n-type sample leading to a wider depletion zone about the cavity layer. In both cases, w drops off noticeably at higher temperatures. In the next section, we will compare our calculated barrier widths with these experimental values.

Figures 5 and 6 illustrate that both the trans-barrier current and the high-frequency capacitance are roughly symmetric for the n-type ohmically contacted samples. Figure 6 shows that application of bias widens the de-

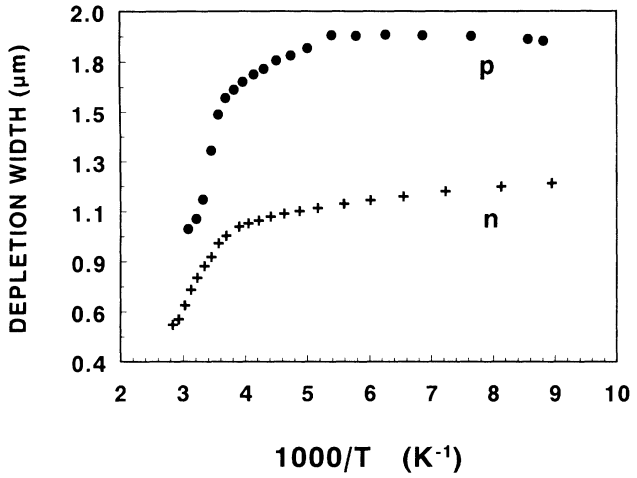

FIG. 4. The depletion layer widths deduced from 1-MHz capacitance at zero dc bias for ohmically contacted n-type (crosses) and p-type (circles) Si samples containing a buried layer of He-implantation-produced nanocavities. The sample electrode areas were 11.6 mm^2.

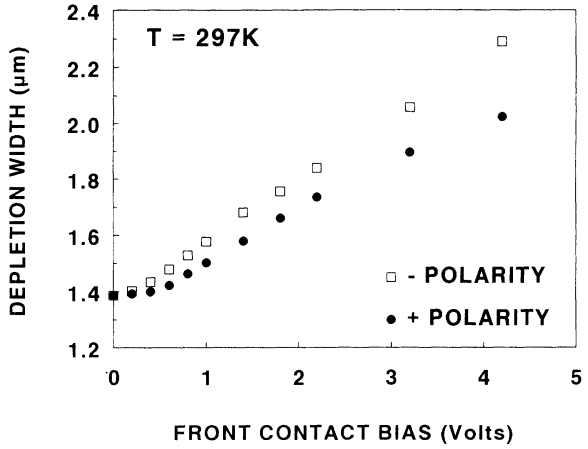

FIG. 6. The depletion layer widths deduced from 1-MHz capacitance versus dc bias on the top gate electrode at 297 K for an ohmically contacted n-type Si sample containing a buried layer of He-implantation-produced nanocavities. The sample electrode area was 11.6 mm^2. The rise of the width with bias is evidence that the negative charge on the cavities increases.

pletion region around the nanocavities. Since it can be readily shown that the net amount of areal charge in these structures must be zero (as long as the depleted regions do not touch the surface), the demonstration that the depletion width grows with bias means that the negative charge density in the cavities must grow as well. We will use this fact later to demonstrate the emission of bias-injected electrons into the conduction band in order to measure the energy level of trapped negative nanocavity charge.

C. Capacitance-voltage measurements

We now discuss the results obtained on the Schottky-barrier samples. Sample structures such as these are commonly used to generate capacitance-transient data which can be analyzed to determine carrier emission rates from gap state electronic levels. In addition to such DLTS analysis, the variation of capacitance with dc bias

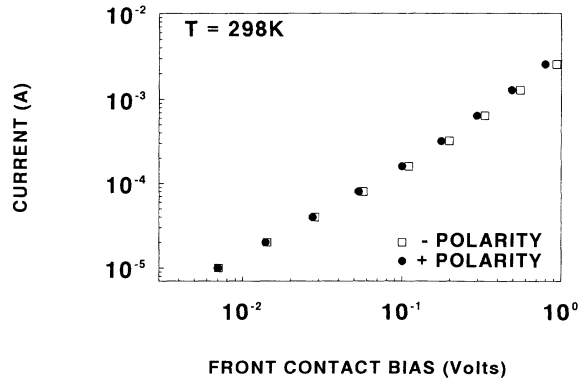

FIG. 5. The dc current versus top gate bias at 298 K for an ohmically contacted n-type Si sample containing a buried layer of He-implantation-produced nanocavities. The sample electrode area was 11.6 mm^2.

can provide information on the depth distribution of electrical centers. In this section, we will treat this problem using the same symbol w for the bias dependent depletion depth that extends from the gate electrode metal that was used for the depletion width surrounding the nanocavity layers in ohmically contacted samples. In some cases, Schottky-barrier biasing causes these two depleted regions to merge, and w then refers to the total depth depleted, measured from the front surface. The analysis used to treat capacitance data from Schottky barriers containing deep levels has been previously discussed.[17] In the case where charge exchange at the small signal, high-frequency test bias only occurs at the depletion edge, and with the proviso that the dc depletion bias does not change the steady-state occupation of the deep states located inside the depletion edge, it has been shown[17] that

$$Q(w)=(2/\varepsilon q)[\partial(1/C)^2/\partial V]^{-1}\,, \tag{15}$$

where $Q(w)$ is the depletion edge charge density, and w is given by the parallel-plate formula [Eq. (14)]. In most practical circumstances, these restrictions are only obeyed over a limited range of bias conditions, and in these cases $Q(w)$ will be identical to the shallow doping density. Information about the deep-level charge density must be obtained from more detailed analyses. First, we will review the experimental capacitance data.

Figures 7–9 show $1/C^2(V)$ plots and plots of $Q(w)$ obtained from Eq. (15) for the n-type Au Schottky-barrier samples at several temperatures and frequencies. We observe that the $C(V)$ and $Q(w)$ curves look very similar at both 1 MHz and 100 kHz at the lowest temperatures, but as T increases, $C(V)$ becomes quite large, particularly at the lower frequency. The low-temperature values of $Q(w)$ are in the middle of the P doping range; we will argue that this is in the range of validity of Eqs. (13)–(15). Note that the smallest values of w shown in these figures exceed the depths where we expect to find any implantation-induced cavities. At higher temperatures

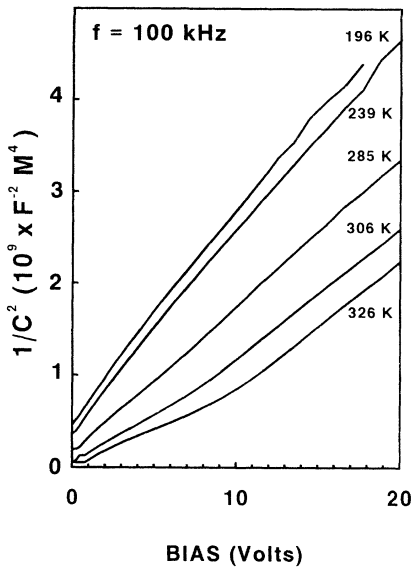

FIG. 7. The inverse square of the 100-kHz capacitance versus reverse gate bias at various temperatures for a Au Schottky-barrier n-type Si sample containing a buried layer of He-implantation-produced nanocavities. The sample electrode area was 4.6 mm^2.

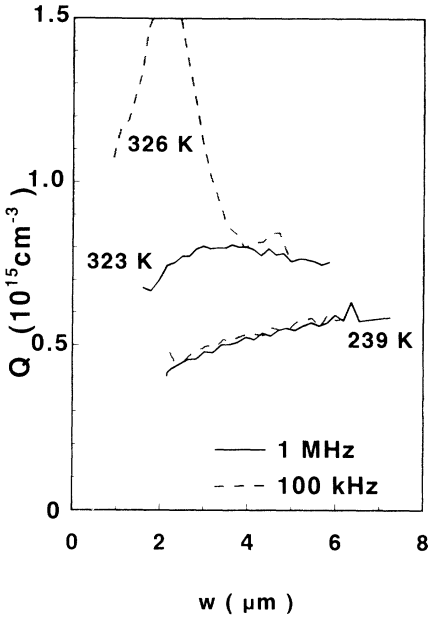

FIG. 9. The effective depletion layer charge density for a Au Schottky-barrier n-type Si sample containing a buried layer of He-implantation-produced nanocavities. This density was deduced from the 100-kHz (dashed line) and 1-MHz (solid line) data of Figs. 7 and 8 using Eq. (15). The sample electrode area was 4.6 mm^2. At the lower temperature the effective charge density is independent of frequency, indicating that the cavity charge is essentially static. At the higher temperatures the cavity charge responds significantly to the rf potential, resulting in the observed frequency dependence. In all cases, the effective charge density approaches the density of P dopants as the depletion edge moves beyond the cavity layer.

we expect that the localized nanocavity states can capture and emit charge at the test frequencies, and the attendant rise in $C(V)$ seems reasonable. In the next section, we will discuss our modeling of the higher-temperature data in some detail. At temperatures lower than ~190 K, measurements of the V dependence of C required inconveniently long dc bias intervals because of the time required to equilibrate the depletion layer charge at each new voltage value.

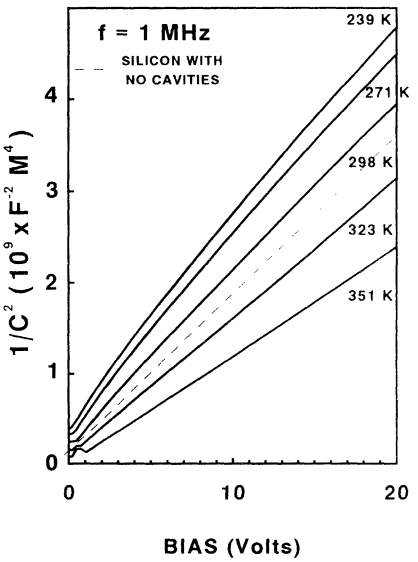

FIG. 8. The inverse square of the 1-MHz capacitance versus reverse gate bias at various temperatures for a Au Schottky-barrier n-type Si sample containing a buried layer of He-implantation-produced nanocavities. The sample electrode area was 4.6 mm^2. The dashed line is an idealized curve generated to simulate the data on a cavity-free silicon sample of the same doping density.

Capacitance data obtained at 1 MHZ on the p-type Al Schottky-barrier samples are shown in Fig. 10. The deviations from behavior expected for a Schottky barrier with no deep levels are even more dramatic than for the n-type samples. As in the case of the n-type samples $C(V)$ is larger at high temperatures, and even at 247 K, the values of $Q(w)$ do not agree with the boron dopant density unless the bias is larger than 25 V (not shown). The question of the sign and location of the localized nanocavity charge in a depleted state awaits a complete treatment of the n-type and p-type data given in Sec. V.

D. Measurements of carrier emission rates

We now discuss our capacitance-transient measurements. These were carried out at 1 MHz to probe the time dependence of depletion widths with maximum accuracy and time resolution. The equilibration time for the Boonton 72 B capacitance meter is ~0.5 msec; the longest time constants that could be conveniently followed were on the order of several hundred seconds. The principal issue to be addressed here involves the type of information to be gained from transient measurements on all four types of samples. We shall see that, in contrast to

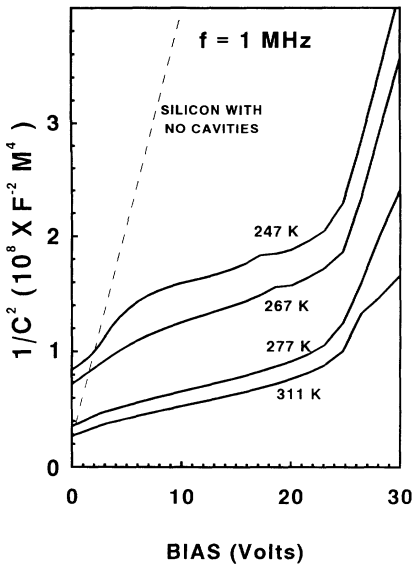

FIG. 10. The inverse square of the 1-MHz capacitance versus gate bias at various temperatures for an Al Schottky-barrier p-type Si sample containing a buried layer of He-implantation-produced nanocavities. The sample electrode area was 4.6 mm^2. The dashed line is an idealized curve generated to simulate the data on a cavity-free silicon sample of the same doping density. The variation of $1/C^2$ from above the no-cavity line reflects the change in sign of cavity charge from positive to negative as the bias is increased. When the depletion edge reaches depths beyond the cavity layer, the slope of $1/C^2$ versus bias reverts to that indicative of the B dopant density.

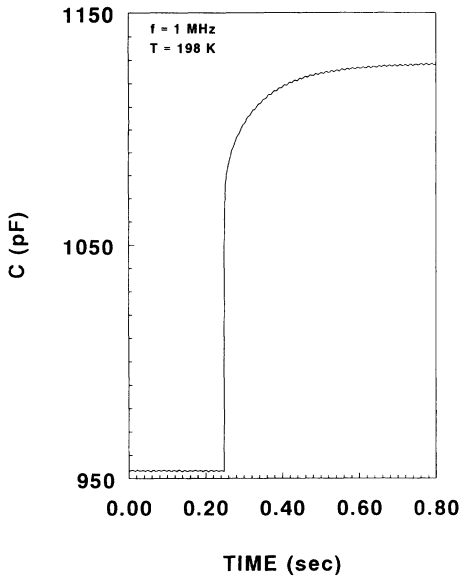

FIG. 11. Capacitance transient measured at 1 MHz on an n-type ohmically contacted sample after a bias change from +1 to 0 V on the front electrode. Sample temperature was 198 K. This transient is believed to reflect electron emission from negatively charged cavities.

the rather symmetrical behavior for n-type and p-type seen in the majority carrier transport behavior, the transient-capacitance studies show a novel but qualitatively understandable asymmetry.

We first discuss the n-type ohmically contacted samples. Because we have shown that small applied biases increase the trapped electron density (deduced from Figs. 5 and 6), it should be possible to observe the relaxation of this bias-injected state and measure an electron emission rate from the nanocavity localized states. The results of such measurements are shown in Fig. 11. Here we have applied a small bias across the potential barrier and watched the depletion layer capacitance relax after the bias is removed. This is an analogous experiment to one carried out on silicon grain boundaries by our group[15] in 1979. The data show that the capacitance relaxes upwards about 15% over the time period of ~0.2 sec after the applied bias is removed. The direction of the capacitance transient confirms that electrons are being emitted, and the potential barrier around the cavities is narrowing. The observed transients are close to first order in time and the deduced rates are plotted versus inverse temperature in Fig. 12. We notice first that the rates are independent of the injection bias direction (compare circles and squares). Secondly, in addition to an emission process characterized by an energy of 0.37 eV, there is also a faster, more weakly activated component observed at lower temperatures. The center producing this component is unknown at present, although the similarity of its energy to the P donor ionization energy, 0.045 eV, suggests a perturbed P center. In this regard, we note that some P atoms within the cavity layer can be expected to reside on the internal surfaces. We shall discuss the emission prefactors obtained from this plot in the next section.

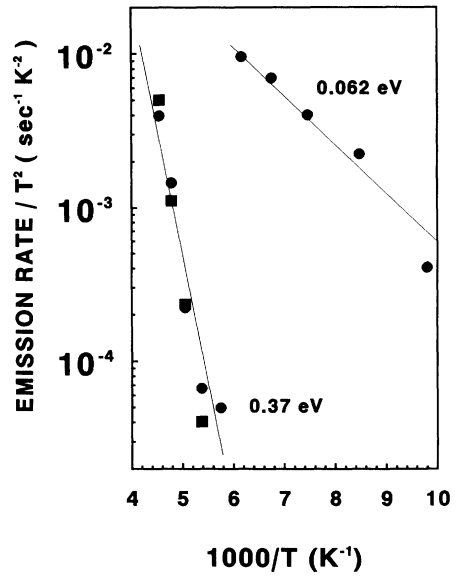

FIG. 12. The measured electron emission rate divided by absolute temperature squared deduced from 1-MHz capacitance transients on n-type ohmically contacted Si samples. Circles are for data obtained after +1 to 0 V transitions; squares are for data obtained after −1 to 0 V transitions. The 0.37 energy is believed due to hole emission as the cavities change from positive to negative charge.

Given that we have *n*-type Schottky-barrier structures where the region of carrier depletion can be extended to depths beyond the cavity layer, it is sensible to attempt a conventional DLTS measurement where the capacitance transient is observed after the application of bias. If the charge change upon going to depletion is in the normal direction observed for isolated point defects (less negative), such a measurement would give a measure of electron emission rates in depletion. Figure 13 illustrates that, in contrast to this simple expectation, the capacitance transient indicates that the depleted state is in fact *more negative*. After the depletion bias is changed from zero to -5 V, C decreases, indicating that electrons are being captured, not emitted by localized states. We also note that the transients observed in this experiment are not composed of single exponential segments but have a more complicated time dependence. We emphasize that the 5-V bias employed here produces carrier depletion depths well beyond the end of the nanocavity zone, and the frequency independence of C in this temperature range (see Figs. 7 and 8) means that we should only be seeing capacitance contributions to charge at the depletion edge. To restate the somewhat novel conclusion of these experiments: it appears that the nanocavities are more negatively charged in depletion. In the next section, we will show that a simple model can also produce this result.

We turn next to transient measurements performed on *p*-type samples. First we note that the *n*-type results show that conventional DLTS measurements on *p*-type samples should probe the emission rate of holes. This follows from the fact that the majority-carrier transport data argues for a positive charge state in equilibrium, and the *n*-type Schottky-barrier transients show that the cavities are negative when fully depleted. Thus the injection of holes at zero bias should be followed by emission of these same species in depletion. The data shown in Fig. 14 appear to support this contention. Here we show a capacitance transient observed after a 0 to 25 V bias step applied to the Al gate of our *p*-type Schottky-barrier devices. C is observed to increase with time after depletion is achieved, indicating a loss of positive charge. Note that a large depletion bias was used to put the sample in the range of data in Fig. 10 where the charge density is representative of the known doping level. The results of several experiments of this type are shown in Fig. 15. The observed emission rates are characterized by an activation energy of only 0.17 eV and the emission rate prefactor is very low, as will be discussed in the next section.

An alternative way to measure hole emission might be to bias the ohmically contacted *p*-type devices and observe the emission of holes at zero bias, as was done for the *n*-type samples. Again we note that the bias dependence of the 1-MHz capacitance indicates that this will inject excess majority carriers into the localized nanocavity states. Figure 16 shows the results of such an experiment at 197 K. C is observed to recover upward just as in the *n*-type case indicating the emission of excess holes. The total change in C is about 10%, indicating that the potential barrier has not been dramatically raised by the application of a 1-V bias. This small change in C means that we must also address the influence of hole capture in our data. We will defer this issue to Sec. V. The data obtained form this experiment are plotted in Fig. 15. Surprisingly, the activation energy seen for this data, 0.71 eV, is much higher than for the Schottky-barrier hole emission measurements. In addition, its prefactor is also very large. We note, however, that if holes and electrons are both trapped in the cavities in equilibrium, hole emission could in principal occur from either the positive or the neutral state of the dangling bond. In the next sec-

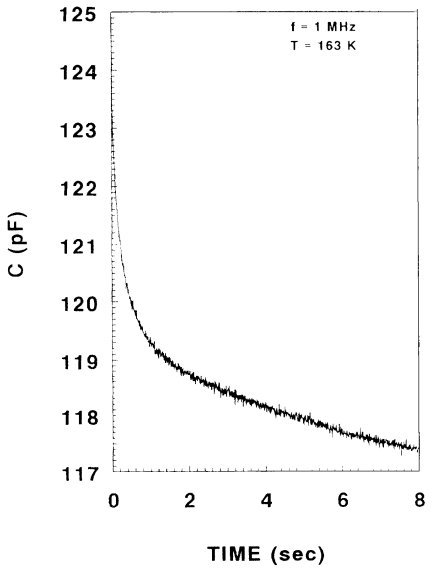

FIG. 13. Capacitance transient measured at 1 MHz after a 0 to -5 V bias transition on a Au Schottky-barrier *n*-type silicon sample at 163 K. The decrease in C indicates that the trapped electron density is larger in the -5-V state.

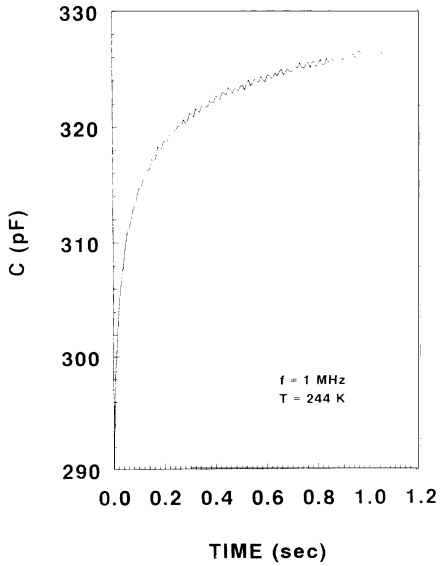

FIG. 14. Capacitance transient measured at 1 MHz and 244 K for an Al Schottky-barrier *p*-type Si sample after a bias transition from 0 to 25 V on the front gate.

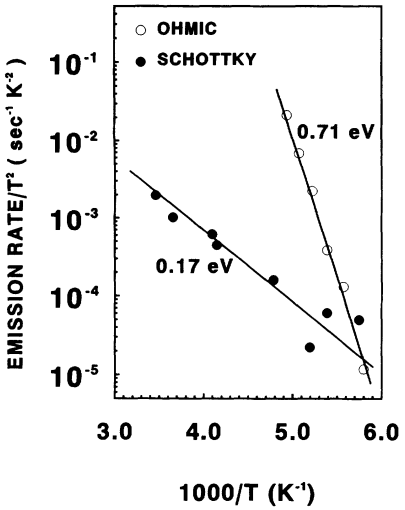

FIG. 15. Measured hole emission rates divided by absolute temperature squared for ohmically contacted and Schottky-barrier p-type samples. The ohmically contacted sample underwent a bias step from -1 to 0 V, and one of its transients is seen in Fig. 16. It yielded the larger activation energy of 0.71 eV, which is tentatively interpreted in terms of hole emission from the neutral state. The Schottky-barrier sample is that represented in Fig. 14. Its transient yielded the activation energy of 0.17 eV, which is ascribed to hole emission from the positive state.

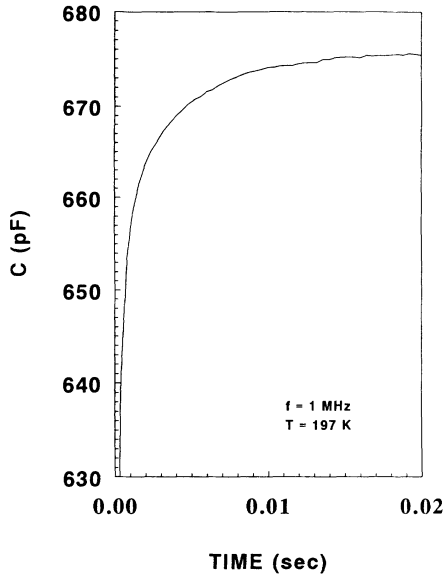

FIG. 16. Capacitance transient measured on an ohmically contacted p-type sample at 197 K after a bias transition from -1 to 0 V on the front contact. The capacitance increases as injected holes are released from the cavity layer, and its depletion width shrinks.

tion, we will in fact propose that the large activation energy reflects the emission of holes from the donor levels located in the upper half of the band gap.

V. DISCUSSION

We now use the simplified mathematical model discussed in Sec. III to interpret, at a semiquantitative level, four types of experiments that were performed on n-type and p-type Si in this study. These are (1) low-bias temperature-dependent conductivity with an ohmic contact, (2), zero-bias capacitance with an ohmic contact, (3) capacitance versus voltage in a reverse-biased Schottky diode, and (4) electron and hole emission rates obtained from capacitance transients. The parameter values used are summarized in Table I. While some are imprecisely known, leading us to round off their values for simplicity, they are sufficiently accurate for the purposes of the present modeling. The approximate cavity-associated donor and acceptor levels are taken from the activation energies for electron and hole emission observed in the present study. The choices are reinforced by their similarity to dangling-orbital donor and acceptor levels reported for the divacancy, which occur at $E_C+0.21$ eV and $E_C+0.73$ eV.[21] Following the approach to Coulomb-repulsion effects within a cavity, which was discussed in Sec. III, we treat the cavity as having one donor and one acceptor level, each with a degeneracy equal to the actual number of dangling bonds on the internal surface. The capture cross sections for electrons and holes at a neutral dangling orbital are multiplied by the degeneracy, thereby taking account of the multiplicity of available charge receptors while precluding the attachment of more than one charge of a given sign. The degeneracy multiplier is not applied to the capture cross sections at charged dangling orbitals, however, since within the model there can only be one such orbital of a given sign in a cavity. The B and P concentrations employed in the calculations are varied from case to case so as to be representative of experimental conditions.

While we do not carry out a detailed treatment of intracavity Coulomb interactions as a function of charging, it is useful to consider the approximate range of these effects in assessing the applicability of the above model. This was accomplished by solving[22] the Poisson equation for a spherical void of diameter 20 nm that contains two electron charges and is embedded within an infinite dielectric continuum with a dielectric constant of 11.9. Two configurations of the charge were considered, one with the electrons on adjacent dangling bonds at the unreconstructed (111) surface, and the other with the electron charges uniformly distributed over the surface of the sphere in the spirit of a mean-field approximation. The electron-electron repulsion energies for these cases are, respectively, 0.58 and 0.012 eV. Thus, the Coulomb-repulsion energy can range from prohibitively large values to values on the order of kT. Consequently, we consider it probable that the 20-nm cavities can actually take on several electron charges under some conditions rather than the one assumed in the modeling. Indeed, preliminary calculations using the above mean-field treatment of intracavity Coulomb repulsion yield a charge per cavity of approximately -3 under conditions of full carrier depletion at a temperature of 300 K. Therefore, as previously emphasized, the modeling should be regarded as semiquantitative.

Figures 17 and 18 show the results of model calcula-

TABLE I. Parameter values at 300 K used in theoretical modeling.

Property	Value	Origin
B [0/−] level	$E_V+0.045$ eV	Ref. 18
P [+/0] level	$E_V+1.075$ eV	Ref. 18
Cavity [+/0] level	$E_V+0.2$ eV	cavity DLTS; also divacancy DLTS[a]
Cavity [0/−] level	$E_V+0.7$ eV	cavity DLTS; also divacancy DLTS[a]
Cavity [+]-state degeneracy	10^4	no. dangling bonds per cavity (TEM)
Cavity [−]-state degeneracy	10^4	no. dangling bonds per cavity (TEM)
σ_n for cavity [+/0] level	10^{-12} cm^2	π[× radius where Coulomb attraction $\sim kT$]^2
σ_p for cavity [0/−] level	10^{-12} cm^2	π[× radius where Coulomb attraction $\sim kT$]^2
σ_p for cavity [+/0] level	10^{-11} cm^2	[atomic spacing]^2×[degeneracy]
σ_n for cavity [0/−] level	10^{-11} cm^2	[atomic spacing]^2×[degeneracy]
Cavity donor state areal density	3×10^{11} cm^{-2}	Areal density of cavities (TEM)
Cavity acceptor state areal density	3×10^{11} cm^{-2}	Areal density of cavities (TEM)
Depth distribution for cavity states	$(8\times10^{15}$ cm$^{-2})\exp[-0.5(x-1.35\ \mu\text{m})^2/(0.15\ \mu\text{m})^2]$	Gaussian approximation of calculated He-implantation profile
Au/n-type Schottky barrier	0.80 eV	Ref. 18
Al/p-type Schottky barrier	0.58 eV	Ref. 18

[a]Reference 21.

tions for n-type and p-type Si that is unbiased and in equilibrium at a temperature of 300 K with an ohmic contact. Note that as anticipated in the introductory discussion in Sec. III, cavity charging results in potential barriers which repel majority carriers in both n-type and p-type silicon. In the case of n type, the negative cavity states are near saturation, while the population of positive states is negligible. In p type, the positive and negative states are both significantly populated, the occupied fractions at the center of the cavity layer being 51% and 28%, respectively. This occurs in spite of the Fermi level being above the [+/0] level and below the [0/−] level because of the large degeneracy assigned to the charged states, which greatly enhances the probability of their being occupied.

Two measurable properties can be extracted from Figs. 17 and 18 for comparison with experiment. One of these is the activation barrier for low-bias majority-carrier current, which is equal to the energy separation between the Fermi level and either the conduction band (n type) or the valence band (p type) at the center of the cavity layer. From Figs. 17 and 18 one obtains barriers of 0.34 eV for n type and 0.44 eV for p type. Experimentally (Fig. 3), we deduce values of 0.19 and 0.26 eV for the activation energy of G/T. We note that the actual formula[19] for E_a is $\phi_B+\zeta-T\partial(\phi_B+\zeta)/\partial T$, and this second term is not only important, but also quite model dependent. Because the calculated value of ϕ_B increases with temperature for n type and decreases for p type, it turns

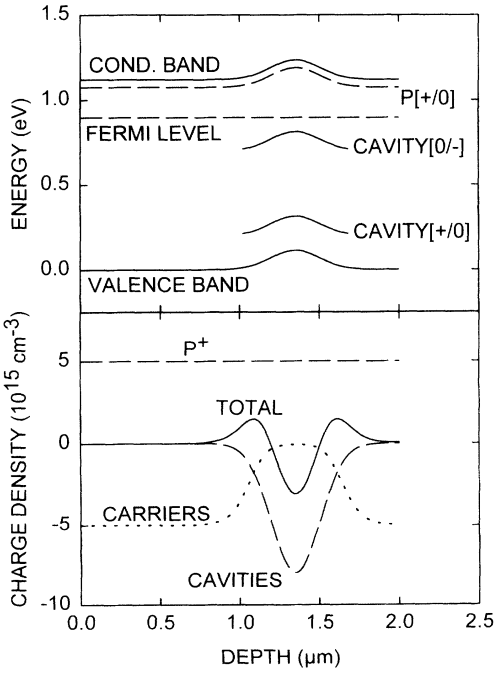

FIG. 17. Band bending and charge densities computed for n-type silicon in equilibrium at 300 K using the simple one-electron model and the parameters listed in Table I. With the Fermi level in the upper half of the band gap, the charges on the cavities are predominantly negative.

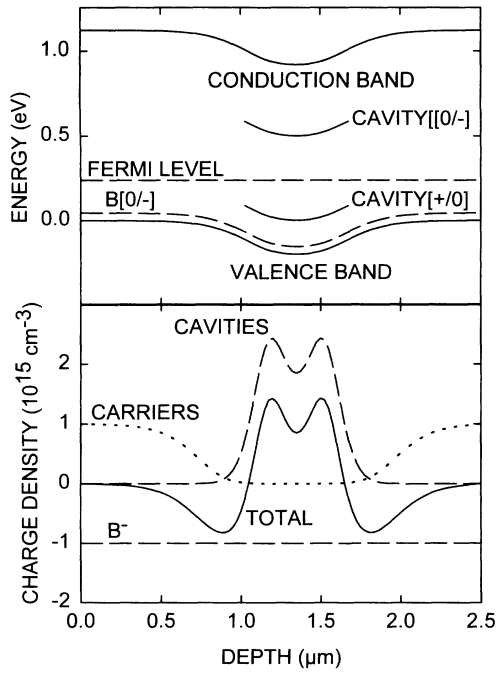

FIG. 18. Band bending and charge densities computed for p-type silicon in equilibrium at 300 K using the simple one-electron model and the parameters listed in Table I. With the Fermi level in the lower region of the band gap, the net charge in the cavity layer is positive, although there is calculated to be appreciable occupation of the negative state at depths where the band bending is most extreme.

out that the predicted value of E_a at high temperatures is ~ 0.034 eV for n type, lower than the calculated $\phi_B + \zeta$, and ~ 0.49 eV for p type, which is higher than the calculated value of $\phi_B + \zeta$. These values bracket the observed high-temperature slopes but do not closely agree with either of them. Our modeling has convinced us that this particular parameter is quite sensitive to the details of the calculation-cavity density, energy levels, etc., so we are not surprised at the semiquantitative level of agreement with theory.

At temperatures below 300 K, the experimental variation of G/T weakens drastically. To understand this behavior we must address the issue of the areal uniformity of the potential barriers in the cavity region. Given the size and density of nanocavities, we would expect that statistically, there must exist regions in the cavity layers where occasional deficits in cavity density and trapped charge will produce low spots in the cavity potential barriers. These regions of "easy" transport for majority carriers will become favored at lower temperatures where the conductance per unit area of the normal regions becomes small. This phenomenon has been seen in grain boundaries shunted by edge damage and also by bulk nonuniformity effects.[23] We note that such low spots are not expected to influence capacitance measurements very much because the capacitive current flow at 1 MHz will still be rather uniformly distributed, and the data of Fig. 4 appear to bear this out. Finally, we note that the experimentally observed weakening of the temperature dependence of G/T ascribed to shunting may partially explain why the experimental activation energies lie below the model predictions.

A second measurable property is the width of the barrier, which we take as the separation of the half-amplitude points for carrier depletion. These calculated widths are plotted as a function of temperature in Fig. 19, and should be compared with the experimentally derived data [using Eq. (14)] in Fig. 4. The qualitative agreement is excellent; the model calculations predict the temperature independence seen at low temperatures and the sharp drop at higher temperatures. This effect is due to the movement of the bulk Si Fermi level towards the center of the band gap. The absolute width values are quite sensitive to the shallow doping levels which were only estimated from the wafer dopant specifications (a range of a factor of 2). Thus, some of the quantitative disagreement in w, particularly for the n-type data might be attributed to this uncertainty. However, it is also clear, particularly for the n-type data, that the theory predicts that the drop in w at higher temperatures will occur at higher temperature than is actually observed.

We turn now to the radio-frequency capacitance of Schottky diodes under reverse bias, considering first the behavior in p-type material. Figure 20 shows a plot of $1/C^2$ versus electrostatic potential at the Si side of the Al/Si interface for a dopant density of 3×10^{15} B/cm^3. The three curves in the figure represent (1) Si without cavity-associated levels, (2) Si with cavities in the low-frequency limit where the cavity levels respond fully to the rf, and (3) the high-frequency limit where cavities conform to the dc bias but respond not at all to the 1-MHz rf. In the absence of cavity effects, the model exhibits the usual linear variation of $1/C^2$ versus bias with a slope that is determined by the dopant concentration according to Eq. (15). When cavities are introduced, the capacitance is modified both by the addition of static

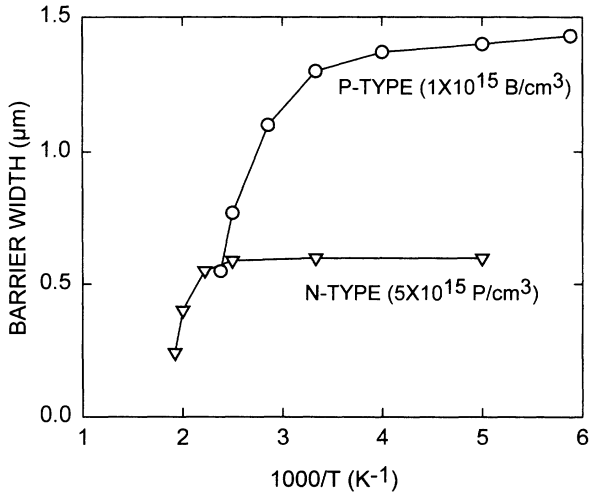

FIG. 19. Depletion layer widths surrounding nanocavity layers computed for n-type and p-type silicon in equilibrium at 300 K using the simple one-electron model and the parameters listed in Table I. Here the width is taken as the depth interval about the cavity layer where the calculated concentration of majority carriers is depleted by more than a factor of 1/2.

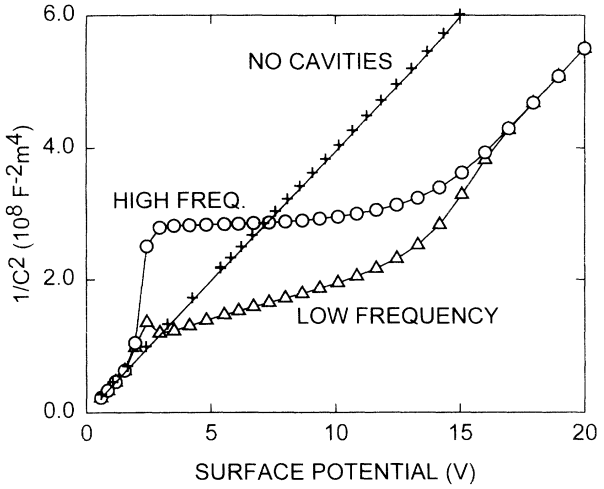

FIG. 20. Theoretical model results for $1/C^2$ behavior expected for Al Schottky-barrier structures on p-type silicon at 300 K using the parameters listed in Table I. In the case of the high-frequency curve the cavity charge was allowed to respond fully to the static bias but not at all to the rf potential, whereas for the low-frequency curve the cavity layer charge followed the rf potential fully, thereby producing a larger capacitance. The variation of computed $1/C^2$ from above to below the values for the no-cavity condition is due to the change in cavity charge from positive to negative with increasing reverse bias. This behavior corresponds to that observed experimentally, as seen in Fig. 10.

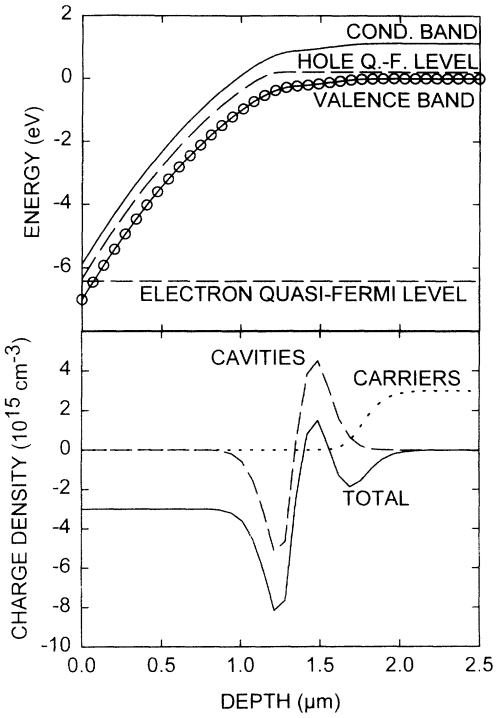

FIG. 21. Band bending and charge densities computed using the simple one-electron model for ~6-V bias on an Al Schottky barrier on p-type silicon containing a nanocavity layer using the parameters listed in Table I. The temperature was 300 K. At this particular bias, approximately 1/2 of the cavity layer has undergone the change from positive to negative charge.

charge (the only effect in the high-frequency limit) and by the response of the cavities to the rf.[17] Depth profiles for a surface potential of 6 V are presented in Fig. 21. At this point the depletion-zone edge is moving through the cavity layer. As a result, the net positive charge present in the unbiased state is giving way to the high-bias condition, in which the depletion zone extends beyond the cavities, and the negative cavity states are nearly saturated while the positive states are virtually unoccupied. In the latter regime, the slope of $1/C^2$ versus surface potential reverts to that of cavity-free material, but the curve is displaced to higher bias by an amount that is approximately proportional to the static charge in the cavity layer.

We can compare these model calculations with the 1-MHZ capacitance data shown in Fig. 10. As we noted previously, the high-bias slopes of the experimental $1/C^2$ curves for these p-type samples yield approximately the correct doping density, particularly at the lowest temperatures, where charge exchange with the cavity localized states is negligible. We see that the general relationship between the sample data in Fig. 10 and the idealized "no-cavity" curve shown in Fig. 20 is much like that predicted from our model calculations. The experimental curves for cavity-containing samples start above the no-cavity curve at low bias, cross this curve, and eventually become parallel to it at large gate biases. The observed displacement between the two curves is about 2.5 times that predicted theoretically (19 versus 7.5 V), and this apparently reflects an underestimate of the amount of negative cavity charges in the fully depleted state. The probable implication of the above comparison is that our previously discussed assumption in the model of no more than one charge per cavity is too restrictive under conditions of bias-induced depletion. If, however, the number of cavity-associated charging sites in the calculation is increased to conform to the variation of capacitance with bias then the previously discussed activation barriers for low-bias conduction in ohmically contacted samples are increased to values substantially larger than experimentally observed. This disparity is believed to arise from our simplified treatment whereby the cavity dangling bonds have only one donor level and one acceptor level with Coulomb repulsion being introduced as an abrupt cutoff in the number of bonds per cavity that can receive charge. In reality, as successive charges are added to a cavity, Coulomb repulsion probably results in several different dopant levels within the band gap. A more elaborate treatment including these multiple levels should accommodate the difference in cavity charging between equilibrium and depletion conditions.

Calculations for n-type Si containing 1×10^{15} P/cm^3 together with cavities are presented in Figs. 22 and 23. The behavior here differs qualitatively from that of p-type because, in the n-type material, the negative cavity charge, which again grows with increasing reverse bias, is opposite in sign to the P dopant. One qualitative consequence is that the capacitance is reduced instead of increased by the cavity charge. Another is that the downward slope of the bands under bias is inhibited over a

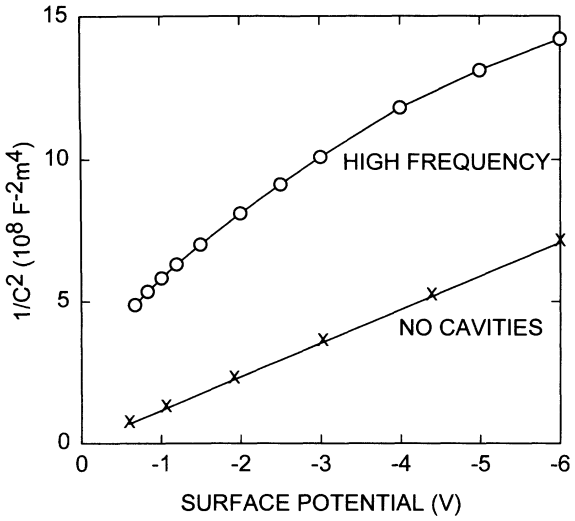

FIG. 22. Theoretical model results for $1/C^2$ behavior expected at 300 K for Au Schottky-barrier structures on n-type silicon using the parameters listed in Table I. In contrast to the situation in the p-type material, the increasing negative charge on the cavities with increasing carrier depletion is now opposite in sign to the change on the P dopants. This leads to the more complicated behavior that is revealed in Figs. 23 and 24.

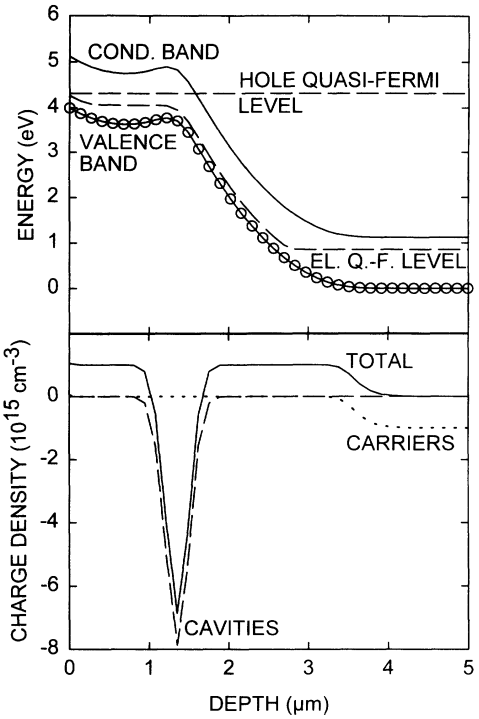

FIG. 23. Band bending and charge densities computed using the simple one-electron model for ~ -3.5-V bias on a Au Schottky barrier on n-type silicon containing a nanocavity layer using the parameters listed in Table I. The temperature was 300 K. The greater complexity of the band bending when the cavities and dopants have opposite sign of charge is apparent.

depth range extending from the surface through the cavity layers, as seen in the upper part of Fig. 23. As a result, the cavity charge is still changing with bias after carrier depletion has occurred at substantially greater depths. This varying cavity charge is reflected by curvature in the plot of $1/C^2$ versus surface potential in Fig. 22. Full depletion in the cavity region is achieved only at very high biases where the slope reverts to that of the Si without cavities, which occurs at a gate bias of about -6 V.

The experimental n-type Schottky-barrier $1/C^2$ data shown in Figs. 6 and 7 shows strong similarities to the model calculations. Again we focus on the low-temperature data where charge exchange with the cavity states at 1 MHz is unlikely. At reverse biases above 10 V the slopes of the $1/C^2$ data agree with the phosphorus doping level at both 1 MHz and 100 kHz. At all biases the experimental curves for cavity-containing samples lie above the idealized no-cavity curves, in sharp contrast to the p-type case. This indicates that, as expected, the cavity charge under strongly depleted conditions is opposite in sign to that of the ionized P donors. Interestingly, the shift between the experimental data and the no-cavity curve is less than is seen for the n-type samples, but closer to the modeling predictions (Fig. 22). The modeling shows that charge occupation in a partially depleted state is sensitive to carrier concentrations and is not just a function of the emission rates of hole and electrons from the two localized cavity levels, and the data appears to bear this out.

We now discuss the results of the transient-capacitance measurements in light of the predictions of the simple model. The modeling data indicate that in equilibrium the cavities in n-type Si should be negatively charged, and that essentially none of the localized states should be positive. Experimentally, we find strong evidence that biasing increases the amount of negative charge in the cavities from the fact that the cavity depletion width grows with applied bias of either direction. Therefore, the relaxation transients after bias injection in the ohmically contacted n-type samples would be expected to give a straightforward measure of the emission rate of electrons from the upper localized state to the conduction band. Even though the changes in potential barrier height are small (we estimate less than 0.1 eV from the capacitance data), we believe, based on some straightforward modeling,[24] that capture processes will not alter the observed C transients by more than a factor of 5. The data in Fig. 12 yield an emission energy of ~ 0.37 eV and a capture cross section of $\sim 1.7\times 10^{-12}$ cm^2 using Eq. (8) and $\alpha = 10^4$. We interpret this as the capture cross section for electrons being captured on a single neutral dangling bond multiplied by the degeneracy factor (10^4); its magnitude is, therefore, quite reasonable for a neutral (non-Coulombic) capture event. Finally, we note that while we have argued that capture effects are not large, they will raise the value of the cross section calculated from the data.

A more conventional DLTS measurement with n-type Schottky samples was not successful because our measurements indicated that reverse bias actually increased the negative charge density on the nanocavities. This surprising result also emerges from the model calculations. It is seen, for example, in Figs. 23 and 24 where the band bending and charge densities are plotted versus depth for a simulated Au Schottky barrier at 3.5-V re-

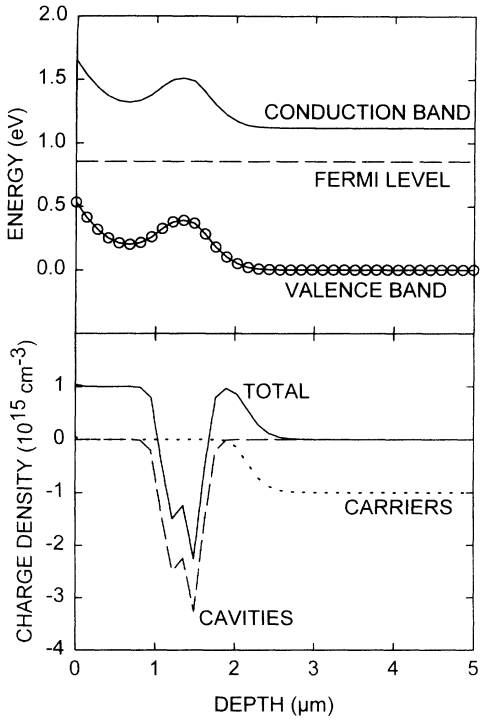

FIG. 24. Band bending and charge densities computed using the simple one-electron model for ~0-V bias on a Au Schottky barrier on *n*-type silicon containing a nanocavity layer using the parameters listed in Table I. The temperature was 300 K. Comparison with Fig. 23 shows the increase of negative charge in the cavity layer with increasing reverse bias, consistent with the experimental results.

verse bias and at 0 bias, respectively. The amount of negative charge is clearly greater in the latter state. The central reason for this effect is that, in equilibrium, the relatively high density of negative cavity charges bends the bands substantially, moving the local Fermi level closer to the valence band. This results in a significant rate of hole capture, which diminishes the negative charge on the cavities. When the reverse bias is applied, the local concentration of holes is progressively reduced, and the cavities become more negative. Such band bending is normally absent in DLTS studies of isolated point defects at low concentrations.

Transient measurements on *p*-type samples yield data which diverge more from the predictions of the simple model. The experiments on Schottky samples (Fig. 15) yield a hole emission energy of 0.17 eV. in calculating a cross section for hole emission from positive dangling-bond orbitals, we again assume $\alpha=10^4$ and use Eq. (9). This yields a capture cross section for holes emitted from the donorlike cavity level of $\sim 2\times 10^{-17}$ cm^2. This should be interpreted (see the discussion preceding Table I) as the cross section for a neutral capture event multiplied by the degeneracy factor; thus, the experimental value is much smaller than we might at first expect. Why is this capture cross section so small? During the capture process, many of the cavities are expected to have trapped electrons. Under these circumstances it is possible that hole capture will preferentially occur on these negatively charged dangling bonds, greatly reducing the effective capture rate on neutral sites.

The second type of hole emission experiment, accomplished by injecting excess holes into the cavity layer in ohmically contacted *p*-type samples, yields an activation energy of ~0.71 eV, much larger than that obtained from the DLTS measurement on *p*-type Schottky barriers. In this experiment, the cavities have a higher hole density than in equilibrium at the start of the capacitance transient. Observation of this rather large energy suggests the possibility that holes are being emitted from the upper (acceptorlike) dangling-bond level; the fact that the energy observed is equal to the difference between E_g and the electron emission energy from the acceptorlike state seems to support this idea. Why should hole emission from the upper state be favored? Our simple model tells us that, before extra holes are injected with bias, both signs of charge exist in the cavity. It seems logical to expect that any injected hole will be more attracted to negatively charged cavities than to positively charged ones. Even if cavities exist with both signs of charge coexisting, an injected hole will prefer to annihilate an electron on the acceptorlike level rather than to exist as a positive charge on the donorlike state. So, we expect that most holes will be captured in the upper state. The degeneracy factor favors hole emission from the upper level as well, since there are roughly 10^4 neutral dangling bonds that can emit a hole, whereas there are only one or perhaps two holes per cavity trapped in the lower (donorlike) state. If we let $\alpha=10^4$ in Eq. (10), we obtain a hole capture cross section of $\sim 6\times 10^{-10}$ cm^{-2}, a very large number. This should be interpreted as the capture cross section for a Coulombic event. Some correction can be made for the lower effective dielectric constant in the vicinity of a cavity, an effect that tends to raise the average attractive electric field of the localized trapped charge. Our rough estimate suggests that this might raise the capture cross section by a factor of 5–10, which still leaves us a factor of ~50 away from the experimental value. However, the scatter in the data does introduce large uncertainties in accurately estimating the emission prefactors, and this remaining discrepancy is not serious when compared with typical DLTS results on deep levels.

It is clear that our simplified theoretical model predicts sizable reductions and enhancements of emission rates, and that these predictions are in semiquantitative agreement with experimental capacitance-transient data. In this regard, we note that the *n*-type emission experiments seem to yield numbers in closer accord with theory than those deduced from *p*-type specimens. We suspect this is because the *n*-type case is inherently simpler, since there are, apparently, only trapped electrons in the cavities. In the *p*-type samples, both signs of carries are trapped. Under these circumstances, an uncorrelated, single-electron approach will be expected to give only semiquantitative predictions of the system properties.

VI. CONCLUSIONS

In this paper, we have examined the electrical behavior of nanocavity-containing layers in *n*-type and *p*-type Si by

a variety of techniques. These cavities were observed to perturb the local band structure strongly, reflecting the influence of the positive, neutral, and negative charge states of the internal surface dangling bonds. Many features of the data were semiquantitatively interpreted in terms of a simplified one-electron model. Moreover, DLTS measurements identified electronic transitions near $E_C-0.37$ eV and $E_V+0.17$ eV that are provisionally assigned to the $[+/0]$ and $[0/-]$ transitions of the surface dangling bonds. These results complement the information on surface electronic states previously obtained from photoelectron spectroscopy of external Si surfaces under ultrahigh vacuum.

Our experiments and theoretical modeling also indicate, however, that at a quantitative level the behavior of such internal surfaces is complex and not amenable to precise description by a one-dimensional, one-electron theoretical model. A major source of this complexity is the strong Coulomb interaction among the charge states of neighboring dangling bonds on the surface, which leads in all probability to a rich spectrum of multielectron states within the cavity. Moreover, the reconstruction of the neutral surface, and the resulting, well-known partial separation of opposing charges to dangling bonds located on inequivalent surface atoms, raises the possibility that excess negative charges and excess positive charges actually reside predominantly on different types of sites, with energy levels displaced appreciably from those of an isolated dangling bond. In addition, the randomly distributed cavities are comparable in size to the Debye length, so that any model based on a continuum with only a one-dimensional spatial variation of properties can provide no more than a first-order approximation. The rather extensive data obtained in this study, therefore, present a challenge to theory which we hope will stimulate further development.

[1]C. C. Griffioen, J. H. Evans, P. C. De Jong, and A. Van Veen, Nucl. Instrum. Methods Phys. Res. Sec. B **27**, 417 (1987).

[2]S. M. Myers, D. M. Follstaedt, H. J. Stein, and W. R. Wampler, Phys. Rev. B **47**, 13 380 (1993).

[3]W. R. Wampler, S. M. Myers, and D. M. Folstaedt, Phys. Rev. B **48**, 4492 (1993).

[4]H. J. Stein, S. M. Myers, and D. M. Follstaedt, J. Appl. Phys. **73**, 2755 (1993).

[5]S. M. Myers, D. M. Follstaedt, and D. M. Bishop, Mater. Sci. Forum **143-147**, 1635 (1994).

[6]D. M. Follstaedt, Appl. Phys. Lett. **62**, 1116 (1993).

[7]D. J. Eaglesham, A. E. White, L. C. Feldman, N. Moriya, and D. C. Jacobson, Phys. Rev. Lett. **70**, 1643 (1993).

[8]See for instance, F. J. Himpsel, Surf. Sci. Rep. **12**, 1 (1990).

[9]R. A. Street and D. K. Biegelsen, Solid State Commun. **33**, 1159 (1980).

[10]P. J. Caplan, E. H. Poindexter, B. E. Deal, and R. R. Razouk, J. Appl. Phys. **50**, 5487 (1979).

[11]E. H. Poindexter, P. J. Caplan, B. E. Deal, and R. R. Razouk, J. Appl. Phys. **52**, 879 (1981).

[12]P. M. Lenahan and P. V. Dresendorfer, Appl. Phys. Lett. **41**, 542 (1982).

[13]See, for example, C. H. Seager, E. L. Venturini, and W. K. Schubert, J. Appl. Phys. **71**, 5059 (1992).

[14]V. V. Kveder, A. E. Koshelev, T. R. Mchelidze, Y. A. Osipyan, and A. I. Shalynin, Zh. Eksp. Teor. Fiz. **95**, 183 (1989) [Sov. Phys. JETP **68**, 104 (1989)].

[15]C. H. Seager, G. E. Pike, and D. S. Ginley, Phys. Rev. Lett. **43**, 532 (1979).

[16]J. F. Ziegler, *The Stopping and Range of Ions in Solids* (Pergamon, New York, 1985).

[17]E. H. Rhoderick and R. H. Williams, *Metal-Semiconductor Contacts* (Oxford University Press, Oxford, 1988).

[18]S. M. Sze, *Physics of Semiconductor Devices* (Wiley, New York, 1981).

[19]G. E. Pike and C. H. Seager, J. Appl. Phys. **50**, 3414 (1979).

[20]W. E. Taylor, N. H. Odell, and H. Y. Fan, Phys. Rev. **88**, 867 (1952).

[21]S. J. Pearton, J. W. Corbett, and M. Stavola, *Hydrogen in Crystalline Semiconductors* (Springer-Verlag, Berlin, 1992), p. 177, and citations therein.

[22]P. M. Richards (private communication).

[23]See, for example, G. E. Pike and C. H. Seager, Adv. Ceram. **1**, 53 (1981).

[24]This conclusion was based on an unpublished calculation of an idealized, zero-width (double-Schottky-barrier) structure for the cavity layer.

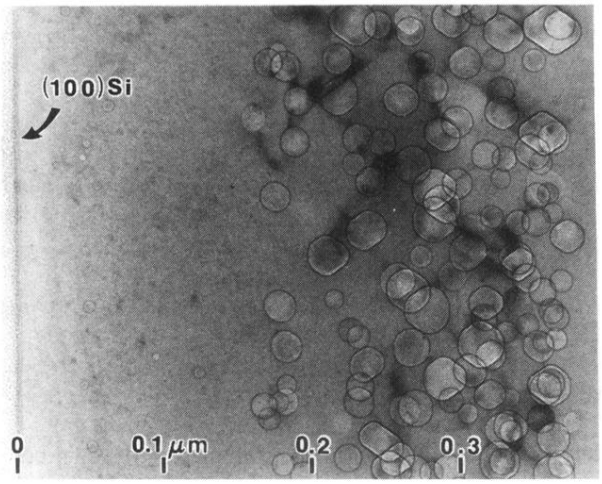

FIG. 1. Cross-sectional ⟨011⟩ TEM micrograph of a (100) silicon sample which has had a 1×10^{17} atoms/cm^2, 30-keV He implant followed by a 900 °C, 1/2 h vacuum anneal. The specimen was tilted to reduce diffraction contrast and imaged at −600 nm under focus to enhance the contrast of the cavities. Clear evidence of faceting is seen.